ACS APPLIED MATERIALS & INTERFACES

Research Article

www.acsami.org

Polylactide-based Magnetic Spheres as Efficient Carriers for Anticancer Drug Delivery

Nikiwe Mhlanga,[†,‡] Suprakas Sinha Ray,[*,†,‡] Yolandy Lemmer,[§] and James Wesley-Smith[†]

[†]DST/CSIR National Centre for Nanostructured Materials, Council for Scientific and Industrial Research, Pretoria 0001, South Africa

[‡]Department of Applied Chemistry, University of Johannesburg, Doornfontein, Johannesburg 2028, South Africa

[§]Materials Science and Manufacturing, Council for Scientific and Industrial Research, Pretoria 0001, South Africa

Supporting Information

ABSTRACT: To improve traditional cancer therapies, we synthesized polylactide (PLA) spheres coencapsulating magnetic nanoparticles (MNPs, Fe_3O_4) and an anticancer drug (doxorubicin, DOX). The synthesis process involves the preparation of Fe_3O_4 NPs by a coprecipitation method and then PLA/DOX/Fe_3O_4 spheres using the solvent evaporation (oil-in-water) technique. The Fe_3O_4 NPs were coated with oleic acid to improve their hydrophobicity and biocompatibility for medical applications. The structure, morphology and properties of the MNPs and PLA/DOX/Fe_3O_4 spheres were studied using various techniques, such as FTIR, SEM, TEM, TGA, VSM, UV−vis spectroscopy, and zeta potential measurements. The in vitro DOX release from the spheres was prolonged, sustained, and pH-dependent and fit a zero-order kinetics model and an anomalous mechanism. Interestingly, the spheres did not show a DOX burst effect, ensuring the minimal exposure of the healthy cells and an increased drug payload at the tumor site. The pronounced biocompatibility of the PLA/DOX/Fe_3O_4 spheres with HeLa cells was proven by a WST assay. In summary, the synthesized PLA/DOX/Fe_3O_4 spheres have the potential for magnetic targeting of tumor cells to transform conventional methods.

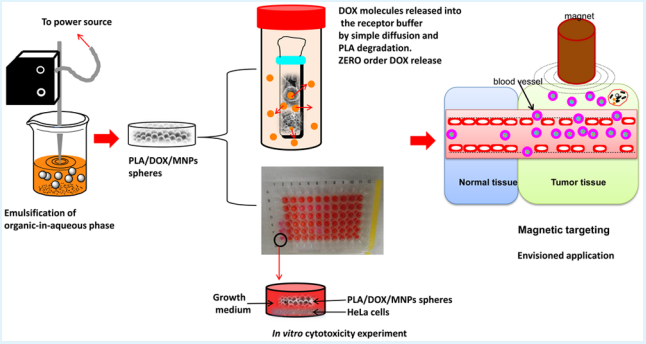

KEYWORDS: *polylactide, Fe_3O_4 nanoparticles, magnetic spheres, anticancer drug, in vitro study, magnetic targeting delivery*

1. INTRODUCTION

As cancer continues to be among the leading causes of human mortality globally, more efficient drug delivery systems are required to revolutionize the present chemo- and radiotherapies. Improvements in targeting include greater specificity to cancer cells, nontoxicity to normal cells,[1,2] and sustained drug release. The idea of magnetic drug targeting (MDT) as an alternative therapy dates back to the 1970s, but to date, only a few MDT treatments have been approved for clinical application by the Food and Drug Administration (FDA).[3,4] MDT entails the conjugation of therapeutics onto the surface of magnetic nanoparticles (MNPs)[5−8] or active targeting through the attachment of high-affinity ligands.[9,10] The unique carrier is directed to the pathological site via external magnetic field modulation.[3,4] Compared with traditional systems, MDT offers optimal controlled drug dosage and tumor cell specificity.[3,11] Importantly, as the deleterious side effects caused by the exposure of normal or healthy cells to toxic drugs are minimized, patient compliance is maintained throughout the treatment.[3,11]

Iron oxide NPs are gaining popularity as vectors for MDT due to their high biocompatibility, small size, ease of preparation, and magnetic properties.[12,13] Superparamagnetic (SPIO) and ultrasmall superparamagnetic (USPION) colloidal iron oxide NPs have already been used in MDT, magnetic resonance imaging (MRI),[14,15] hyperthermia studies,[16,17] biosensing,[18] and detoxification of biological fluids.[19] However, in their pristine state, they tend to aggregate due to their large surface-to-volume ratio and dipole−dipole interactions.[20] To prevent this, their surface has to be modified to mitigate agglomeration and attain colloidal stability in biological environments, particularly to increase plasma half-life and to circumvent the reticuloendothelial system (RES).[11,12,20] A number of stabilizers ranging from polymers to bioactive materials have been used to attain colloidal stability of NPs,[13] and some of these, for example, dextran-coated SPION, have already been approved for clinical use by the FDA.[21,22]

Several studies have applied Fe_3O_4 NPs and biodegradable polymers in anticancer drug delivery applications. For example, Li et al.[23] reported that the anticancer drug curcumin loaded into magnetic poly(lactic acid) microspheres resulted in the sustained release of the drug in simulated physiological blood.

Received: August 17, 2015
Accepted: September 21, 2015
Published: September 21, 2015

DOI: 10.1021/acsami.5b07567
ACS Appl. Mater. Interfaces 2015, 7, 22692−22701

Jia et al.[24] also found sustained release of the relatively toxic doxorubicin (DOX) encapsulated with Fe_3O_4 NPs within biodegradable poly(lactic-*co*-glycolic acid) (PLGA) spheres during in vitro studies. They also tested the cytotoxicity of the carrier in vitro on murine Lewis lung cancer carcinoma cells, in which it induced apoptosis. The DOX-magnetic NP spheres showed even higher antitumor activity in vivo in mice injected with murine LLC cells into their backs than free DOX in the presence of an external magnetic field (neodymium iron boron).

In this study, a single-step emulsion evaporation method involving the coencapsulation of Fe_3O_4 NPs (MNPs) and a model anticancer drug (DOX) into a PLA matrix was used to prepare hybrid spheres. The synthesized Fe_3O_4 NPs were made hydrophobic by coating with oleic acid, which has been reported to further enhance the magnetic properties of Fe_3O_4.[25] DOX is an anthracycline antibiotic that was originally produced by *Streptomyces peucetius var. caesius*.[26] DOX exerts its cytotoxic effect as a DNA-intercalating agent to inhibit further DNA and RNA biosynthesis.[27] Therefore, DOX has been widely used independently or in combination with other chemotherapeutic regimes for various types of solid tumors.[24,28] However, dose-limiting toxic side effects, such as cardiotoxicity, myelosuppression, mucositis, and alopecia, limit the clinical application of DOX due to nonspecific distribution in healthy tissues. Therefore, recent studies have focused on the development of targeted drug delivery systems and administration.

This study investigated the application of PLA, in contrast to the extensively used hydrophobic PLGA, which is a copolymer of PLA and polyglycolide.[24,29−32] PLA is a biodegradable, biocompatible, and bioabsorbable thermoplastic polyester approved by the U.S. FDA for clinical application. PLA can easily degrade under physiological conditions by simple hydrolysis of the ester backbone, and its degradation products are easily excreted through the kidneys or eliminated in the form of carbon dioxide and water through metabolic processes in animals. In addition, PLA exhibits surface erosion, and this property is extremely important for the development of a controlled delivery system (especially for cancer drugs) because the kinetics of surface erosion and the rate of drug release must be highly reproducible.

Both synthesized and OA-modified MNPs were used for the preparation of DOX-loaded PLA/Fe_3O_4 NP spheres. The magnetism of the Fe_3O_4 NPs was measured using a Lake Shore VSM. The physicochemical properties of the spheres were characterized in terms of chemical structure, surface charge and morphology, Fe_3O_4 NPs and DOX loading content. The in vitro release profiles of DOX from the spheres were studied in both acidic and basic environments, and various mathematical models were used to elucidate the release mechanism of DOX from the spheres. WST assay tests were conducted to study the proliferation of human epithelial carcinoma (HeLa) cells. Finally, the uptake of Fe_3O_4 NPs by the HeLa cells was visualized using a transmission electron microscope.

2. EXPERIMENTAL SECTION

2.1. Materials. PLA (PLA2002D) was supplied by Nature Works LLC (Minnetonka, MN). Characteristically, it has ∼4 wt % D-isomer, a weight-average molecular weight of 235 kg/mol, a 1.24 g/cm^3 density, a glass transition temperature (T_g) of ∼60 °C and a melting point (T_m) of ∼153 °C. Analytical standard DOX; anhydrous ≥99.8%, 50−150 ppm amylene stabilizer, total impurities ≤0.001% water dichloromethane (DCM); ≥ 99.9% anhydrous chloroform ($CHCl_3$); dialysis bags with an average flat width of 35 mm (1.4 in.) and MWCO 12 000 Da pore size; phosphate buffer solution (1.0 M, pH 7.4); acetate buffer solution (pH 4.6 ± 0.2); 97% reagent grade iron(III) chloride ($FeCl_3$); 99.99% trace metal basis iron(II) sulfate ($FeSO_4$), ACS reagent, 28−30% NH_3 basis ammonium hydroxide solution (NH_4OH); and greater than 99% hydrolyzed poly(vinyl alcohol) (PVA) were all purchased from Sigma-Aldrich, South Africa. The solvents were used as received without further purification. HeLa cells were purchased from the American Type Culture Collection (Manassas, VA). WST quick cell proliferation assay kit II was received from BioVision (Milpitas, CA). Dulbecco's minimal essential medium (DMEM), 1% (w/v) nonessential amino acids and 1% (w/v) glutamine; trypsin 0.25% EDTA; and penicillin-streptomycin-neomycin (PSN) antibiotic mixture were supplied by Thermo Fisher (Waltham, MA). Standardized fetal bovine serum (FBS), EU-approved and heat inactivated, was supplied by Gibco (Gaithersburg, MD).

2.2. Synthesis of Fe_3O_4 NPs by Coprecipitation Method. Colloidal NPs used for clinical application are mainly synthesized by the coprecipitation method, predominantly because it is the simplest and most efficient method.[12,20] The ferric and ferrous salts were coprecipitated in a 2:1 ratio in aqueous basic media (NH_4OH), with continuous mechanical stirring at 60 °C. The resulting black NPs were filtered, washed with distilled water and ethanol, and subsequently dried at 60 °C in a vacuum oven, modified from the method of Ma et al.[33]

2.3. Synthesis of Fe_3O_4−OA NPs. Hydrophobic Fe_3O_4 NPs were prepared by adding oleic acid to the precipitation of ferric and ferrous salts prepared in the previous steps, modified from Zhang et al.[34] The Fe_3O_4−OA NPs were filtered, washed and dried in a vacuum oven at 60 °C.

2.4. Encapsulation of Fe_3O_4 NPs and DOX into PLA Spheres. The classical solvent evaporation oil-in-water (o/w) emulsion technique was used for the preparation of PLA/DOX/Fe_3O_4 and PLA/DOX/Fe_3O_4−OA spheres. For the preparation of PLA/DOX/Fe_3O_4 spheres, 1 mg of DOX, 100 mg of PLA, and 4 mg of Fe_3O_4 NPs were suspended in 20 mL of volatile solvent, either DCM or $CHCl_3$, providing an oil phase. This oil phase was subsequently introduced into an aqueous phase consisting of 0.1% (w/v) PVA and ultrasonicated for 10 min by means of an UP400s horn at ambient temperature. Subsequently, the oil and aqueous phases were mechanically stirred at ambient temperature for 3 h to evaporate the solvents. The resulting spheres were separated, washed with distilled water and ethanol using a centrifuge, and freeze-dried for storage. The PLA/DOX/Fe_3O_4−OA spheres were synthesized using a similar approach but with a few modifications. The organic phase was prepared by suspending 2 mg of DOX, 100 mg of PLA (as above) and 4 mg of Fe_3O_4−OA in 3 mL of DCM, which was then added to 0.2% (w/v) PVA and ultrasonicated for 10 min in an ice bath.

2.5. Study of DOX Encapsulation Efficacy. The percentage encapsulation efficacy (% EE) of the drug within the spheres was measured after dissolving ∼3 mg of sample in 5 mL of DCM, determining the DOX concentration using UV−vis spectroscopy at λ_{ex} = 485 nm and using the following formula:

$$\%EE = \left(\frac{\text{amount of DOX in spheres}}{\text{amount of feeding DOX}}\right) \times 100 \quad (1)$$

2.6. In Vitro Drug Release Kinetics. To study the in vitro kinetics of the release of DOX from the PLA/DOX/MNP spheres, two pH levels were simulated, namely, physiological blood (7.4, using phosphate buffer) and endosomes (4.6, using acetate buffer). In each drug release experiment, approximately 2 mg of freeze-dried spheres was sealed in dialysis bags with 2 mL of donor buffer. The sealed dialysis bags were immersed into 30 mL of receptor buffer in tubes. The tubes were capped and shaken at 200 rpm horizontally in a JULABO SW22 water bath at 37 °C. At predetermined time intervals (every 2 h for 8 h on the first day and 24 h intervals for the rest of the experiment), 4 mL of the receptor donor was sampled and replaced with the same amount of fresh buffer. The concentration of DOX released was analyzed using UV−vis spectroscopy at λ_{ex} = 480 nm.

DOI: 10.1021/acsami.5b07567
ACS Appl. Mater. Interfaces 2015, 7, 22692−22701

Data obtained were fitted to mathematical models (Supporting Information) that determine and explain the mechanism of the drug release from the system.

2.7. In Vitro Cytotoxicity of PLA/DOX/MNPs. The HeLa cells were maintained and cultured according to routine cell culture procedures. The cells were cultured at 37 °C and 90% humidity in a 5% CO_2 (g) atmosphere in complete medium [DMEM (1% (w/v) nonessential amino acids, 1% (w/v) glutamine), and 10% (v/v) FBS]. The cytotoxic effect of Fe_3O_4, Fe_3O_4−OA, free DOX and PLA/DOX/MNP composites was determined using a WST quick cell proliferation assay kit II, which was performed according to the manufacturer's instructions. The assay is based on the cleavage of the tetrazolium salt, forming formazan by cellular mitochondrial dehydrogenase. Therefore, the amount of dye produced via the activity of dehydrogenase is directly proportional to the number of living cells. The assay was performed in quadruplicate as follows: HeLa cells were seeded in 96-well plates at a density of 1×10^6 cells/well in 100 μL of complete medium [DMEM, 10% (v/v) FBS]. The plates were incubated for 24 h to attain 70−80% confluence. Subsequently, the cells were exposed to different concentrations (0.1, 0.01, and 0.001 mg/mL) of the metal oxides, DOX and spheres and incubated in a 90% humidity atmosphere. After 24 h, each well was washed 3 times with 100 μL PBS and filled with 100 μL complete medium and 10 μL of assay medium. The plates were shaken gently to mix the contents and incubated for 1 h at 37 °C. A Tecan plate reader at 492 nm (measurement wavelength) and 620 nm (reference wavelength) was used to measure the plates' absorbance.

2.8. TEM Imaging of the HeLa Cells Treated with the PLA/DOX/Fe_3O_4 Spheres. To study the uptake of the carriers/NPs, we seeded 1×10^6 HeLa cells into 96-well plates using the same protocols for in vitro cytotoxicity studies. The cells were treated with 0.1 mg/mL PLA/DOX/Fe_3O_4 carrier (8 wells). The plates were incubated for 48 h as in the above section, harvested into Eppendorf tubes and pelleted. The pellets were prefixed in 2.5% glutaraldehyde in 100 mM phosphate buffer (pH 7.2) for an hour. After washing with phosphate buffer, they were postfixed in 1% osmium tetroxide in 100 mM phosphate buffer for an hour. Subsequently, they were dehydrated using a graded series of ethanol solutions, infiltrated with epoxy resin and cured in an oven using conventional techniques. Ultrathin sections (c. 70 nm) of HeLa cells were obtained using a Leica Ultramicrotome, mounted on 200 mesh Cu grids and imaged unstained using a JEOL-JEM 2100 high-resolution transmission electron microscope (HRTEM).

2.9. Characterization. The surface topography and focused ion beam (FIB) cross sections of the spheres were imaged using a Zeiss Auriga field-emission scanning electron microscope (FESEM, Zeiss, Germany). Elemental analysis and mapping were done using an Oxford EDS system fitted on that instrument. HRTEM was used to study the morphology of the Fe_3O_4 NPs supported on holey carbon-coated grids. The crystallinity of the MNPs was studied using a PANalytical X'pert Pro X-ray diffractometer (PANanlytical, The Netherlands). The system was operated with the subsequent settings: 2 theta = 5° start angle and 80° end angle; step size of 0.026; 61.20 time per step; 0.1099419 scan speed; and 11 min 59 s exposure time. A PerkinElmer Spectrum 100 FTIR spectroscope (PerkinElmer, Waltham, MA) was used to attain spectra between 4000 and 400 cm^{-1} wavenumbers at a 4 cm^{-1} resolution. Magnetic properties of the Fe_3O_4 NPs were measured using a Lake Shore Vibrating Sample Magnetometer (VSM). The stability of the materials was measured using a Malvern Zetasizer Nano series (Nano-Zs, Malvern, U.K.). The MNPs and spheres were dispersed in distilled water and adjusted to desired pH levels (2, 4, 6, 8 and 12) using NaOH and HCl solutions. Measurements were recorded at 25 °C. The zeta potential was calculated using Smoluchowski's model. The drug content in the spheres and release medium was measured using a PerkinElmer Lambda 7500 Ultraviolet and Visible (UV−vis) spectrometer (PerkinElmer, Waltham, MA). The absorbance of the 96-well plate was read using a F500 Tecan plate reader at 492 nm and a 620 nm reference wavelength. The average size of the spheres from SEM images was measured using pro premier analyzer software. The diameters of the spheres were measured (≥20 spheres), both smaller and larger ones.

3. RESULTS AND DISCUSSION

3.1. Structure and Morphology of MNPs. The structure of MNPs was characterized using XRD. Powder XRD patterns for Fe_3O_4 and Fe_3O_4−OA NPs, Figure S1 (Supporting Information), respectively, confirmed crystalline phases in synthesized NPs. In the diffractograms, the 2-theta peaks appearing at 30, 36, 44, 57, 63, and 74° are respectively assigned to the 220, 311, 400, 511, 440, and 620 planes, matching standard bulk Fe_3O_4 JCPS no.79-0416, and are in agreement with Qu et al.[35] The crystallite sizes calculated from the peaks (2θ = 36°) were 11.4 and 18 nm for Fe_3O_4 and Fe_3O_4−OA, respectively. With the inclusion of the oleic acid coating onto the surface of the Fe_3O_4, the size increased to 18 nm, endorsing the inclusion of a coating on the Fe_3O_4 surface.

The morphology and size of the synthesized MNPs were evaluated using TEM and SEM. Expectedly, synthesized MNPs tend to aggregate due to their large surface-to-volume ratio and dipole−dipole interaction (Figure 1a), which underscores the need for surface modification to render colloidal stability and improve dispersity.[20] The oleic acid coating minimized the agglomeration of the MNPs, as evidenced by the semi-agglomerated MNPs (Figure 1b).

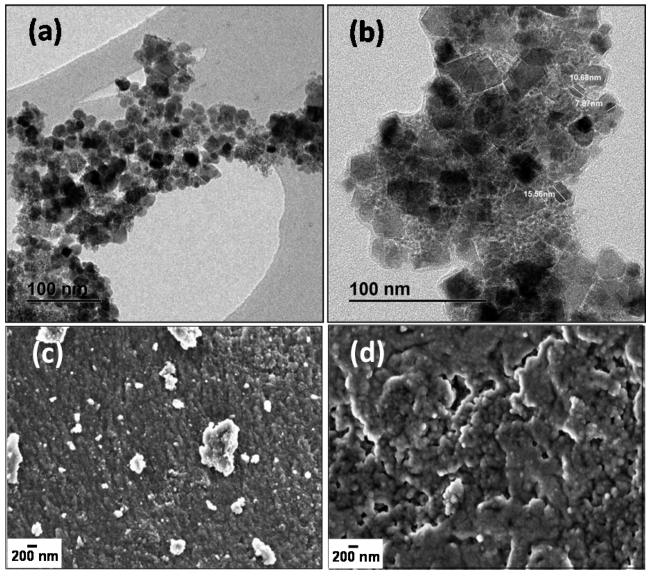

Figure 1. High-resolution transmission and scanning electron micrographs of (a and c) Fe_3O_4 and (b and d) Fe_3O_4−OA nanoparticles. The oleic acid coating increased the size and improved the Fe_3O_4 dispersion.

The average sizes of the Fe_3O_4 and Fe_3O_4−OA NPs measured using TEM were 11 ± 4.52 and 18 ± 1.71 nm, respectively, which agrees with XRD (2θ = 36°, Supporting Information) crystallite size measurements of 11.4 and 18 nm for Fe_3O_4 and Fe_3O_4−OA, respectively. The increase in the size of the Fe_3O_4−OA NPs was due to the oleic acid coating; Lan et al.[36] observed the same trend. Dense packing of Fe_3O_4 NPs resulted in an apparent continuous layer in the SEM image (Figure 1c), whereas individual particles were more visible after coating with oleic acid (Figure 1d), suggesting decreased aggregation.

DOI: 10.1021/acsami.5b07567
ACS Appl. Mater. Interfaces 2015, 7, 22692−22701

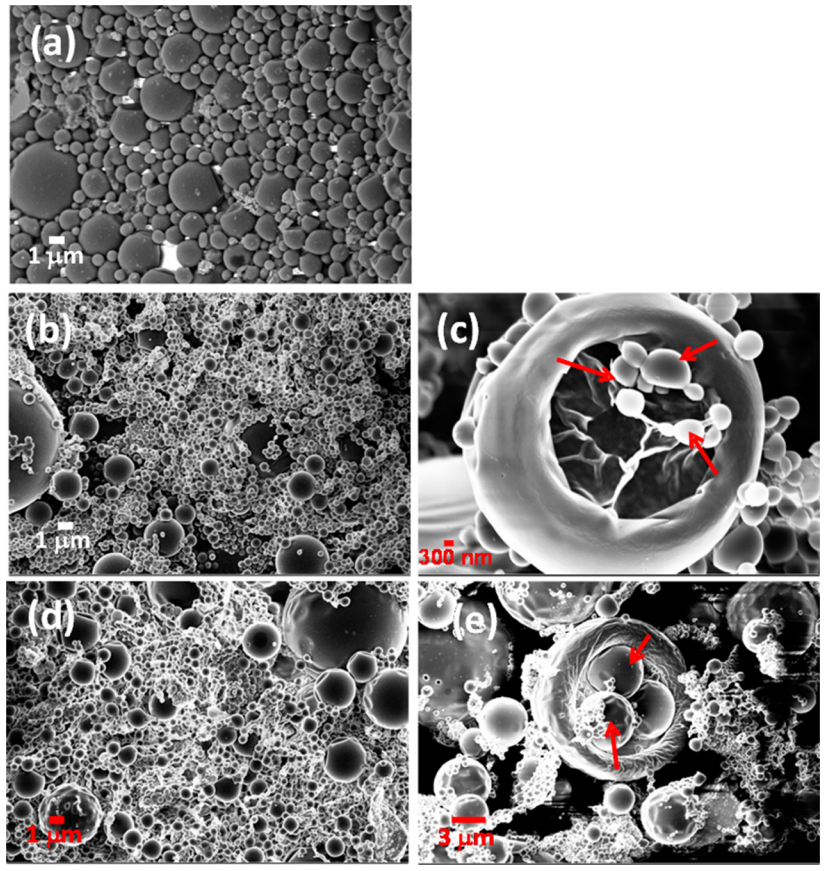

Figure 2. Scanning electron microscopic images of (a) PLA/DOX/Fe_3O_4−OA spheres synthesized in DCM, (b and c) PLA/DOX/Fe_3O_4 spheres synthesized in DCM, and (d and e) PLA/DOX/Fe_3O_4 spheres synthesized in $CHCl_3$.

3.2. Magnetic Property. The magnetism of synthesized Fe_3O_4 was studied using a Lake Shore VSM and a magnet at room temperature. The VSM hysteresis loop for the NPs is shown in Figure S2 (Supporting Information). The magnetization saturation for Fe_3O_4 was 17.904 emu/g. The size, method of synthesis, and shape possibly influence the magnetization. Particles smaller than 20−30 nm are reported to have lower superparamagnetism,[37] which explains the lower magnetism of the Fe_3O_4 NPs, which are approximately 11 nm in size. Furthermore, they had a coercivity (Hei) of 21.874 G, a $30.805E^{-3}$ squareness, and a remanence of 0.51903 emu/g. The NPs were also subjected to a magnetic field at room temperature, and pictures were taken in the absence or presence of a magnetic field (Figure S3, Supporting Information). Magnetism was displayed only in the presence of the magnetic field. This was because the remanence measured using VSM was very low. For magnetic targeting, the carriers are modulated to the site of preference by the inclusion of a magnetic field, and upon reaching the site, the magnetism of the iron oxide is not required. This implies that loss of magnetism in the absence of a magnetic field is a good property for drug delivery applications. Typically, MNPs with diameters less than 30 nm possess superparamagnetic properties at room temperature.[38]

3.3. Sphere Morphology. The present study prepared PLA-based spheres coencapsulating the anticancer drug DOX and MNPs for the MDT of tumor cells to improve traditional therapies. The morphology and size of the synthesized PLA/DOX/MNP spheres were evaluated using SEM. Figure 2 shows the SEM images of the PLA/DOX/MNP spheres. The calculated sizes (using ImageJ software) of the spheres were 0.8 ± 1.3, 0.5 ± 0.6, and 0.6 ± 0.6 μm for PLA/DOX/Fe_3O_4−OA (DCM; Figure 2a), PLA/DOX/Fe_3O_4 (DCM; Figure 2b,c), and PLA/DOX/Fe_3O_4 ($CHCl_3$; Figure 2d,e) spheres, respectively (Table 1). It can be seen that the former spheres (prepared with Fe_3O_4−OA) had a bigger size compared to the latter spheres (prepared with Fe_3O_4); this is due to the additional oleic acid coating on the Fe_3O_4 surface. In the case of the PLA/DOX/Fe_3O_4 spheres, there was almost no influence of the nature of the solvent on the obtained sphere sizes. In some instances, it was possible to observe smaller spheres seemingly encapsulated within microspheres, as shown by the red arrows in Figure 2c,e. In addition to minimizing agglomeration, the PLA matrix is also reported to minimize toxicity by enveloping toxic drugs, attain controlled and sustained drug release, degrade in a biocompatible manner and evade opsonization, which can hinder the delivery of drug to tumor sites.[12,21]

Table 1. Sphere Size and Percentage Encapsulation Efficacy of the Drug within Spheres[a]

PLA/DOX/MNPs spheres	size μm ± std	% EE ± std
PLA/DOX/Fe_3O_4 (DCM) spheres	0.5 ± 0.6	57.5 ± 54.4
PLA/DOX/Fe_3O_4 ($CHCl_3$) spheres	0.6 ± 0.6	59 ± 26.9
PLA/DOX/Fe_3O_4−OA spheres	0.8 ± 1.3	59 ± 43.8

[a]The standard deviation value suggests that spheres of different sizes were prepared, ranging from nanospheres to microspheres.

DOI: 10.1021/acsami.5b07567
ACS Appl. Mater. Interfaces 2015, 7, 22692−22701

3.4. FTIR and EDS Analyses. The inclusion of oleic acid on the Fe_3O_4 NPs was also supported by FTIR analysis. Figure 3 shows the functional groups of the Fe_3O_4, Fe_3O_4−OA, DOX, PLA, and PLA/DOX/MNP spheres. Uncoated Fe_3O_4 showed functional groups typical for pure Fe_3O_4, free of OH groups δ(3401 cm^{-1}) from adsorbed moisture, and Fe−O ν(583, and 431 cm^{-1}), as reported previously.[39,40] Andrade et al.[41] assigned 590 and 450 cm^{-1} to magnetite and maghemite, respectively. Fe_3O_4−OA spectra evidently display inclusion of C−H $\nu_a\nu_s$(2925, 2844 cm^{-1}) from oleic acid. The characteristic Fe_3O_4 peak appearing at 1627 cm^{-1} shifted to 1526 cm^{-1} in Fe_3O_4−OA, and the shift is associated with the combination of C═O with Fe atoms. The observed trend of Fe_3O_4−OA NPs is in accordance with the observation of Lan et al.,[36] namely, the strong CH_2 bands at 2924 cm^{-1} (ν_a C−H), 2853 cm^{-1} (ν_s C−H), and 1405 cm^{-1}(δ_s C−H). The DOX characteristically showed N−H, ν_s(3450 cm^{-1}) and δ(1618, 1521 cm^{-1}); OH groups, ν_s(3330 cm^{-1}); C−H, ν_s(2910 cm^{-1}); C−O, ν_s(1730 cm^{-1}); C−C, ν_s(1410 cm^{-1}); and C−O−C, ν_s(1270, 990 cm^{-1}), in line with the observation made by Kayal et al.[42] PLA typically showed C−H, ν_a(2996 cm^{-1}), ν_s(2935 cm^{-1}), δ(1445, 1365 cm^{-1}); C═O, ν(1749), from the ester bond; and C−O−C, $\nu_a\nu_s$(1181, 1090 cm^{-1}). The PLA/DOX/MNP spheres displayed the same functional groups but with overlapping PLA and DOX peaks, which further supports the inclusion of DOX into the PLA-based spheres. The formation of DOX encapsulated PLA/MNP spheres was further supported by EDS analysis. The EDS spectra for Fe_3O_4, Fe_3O_4−OA, and PLA/DOX/MNPs are shown in Figure S4, Supporting Information. The higher carbon intensity of PLA/DOX/Fe_3O_4−OA was due to the presence of the extra oleic acid coating on the Fe_3O_4 surface.

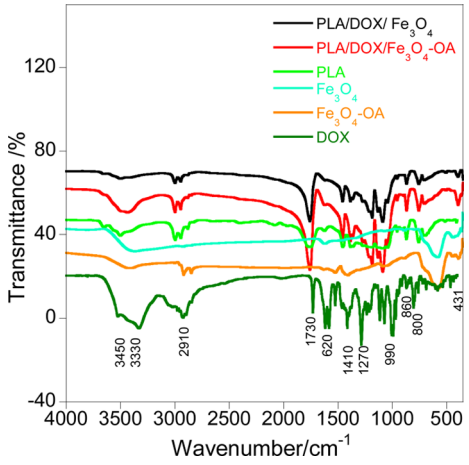

Figure 3. FTIR spectra of PLA, DOX, MNP, and PLA/DOX/MNP spheres. The PLA/DOX/MNP spectra showed PLA, DOX, and MNP functional groups, confirming encapsulation.

3.5. Zeta Potential Measurement. The zeta potential (ξ) determines the cellular interactions of the carriers and the environment to which they are exposed.[43] Figure 4 details the ξ of Fe_3O_4, Fe_3O_4−OA and PLA/DOX/MNPs with a change in pH from basic to acidic. A shift from positive to negative ξ with an increase in pH was observed, especially for Fe_3O_4−OA and PLA/DOX/Fe_3O_4 compared with Fe_3O_4. In contrast, when PLA/DOX/Fe_3O_4−OA was compared with Fe_3O_4−OA, ξ shifted to lower values only at lower pH values (2 and 4) and increased with increasing pH. The shift observed suggests the incorporation of additional compounds into the pure Fe_3O_4. Xu[44] reported that materials with ξ values higher than 25−30 mV are stable; in line with this prediction, our compounds showed stability at basic pH. The inclusion of oleic acid coating and PLA enhanced the stability of the bare Fe_3O_4. Steric stabilization of ceramics using polymers is reported to attain stability, decrease toxicity, and lower agglomeration.[45] Inorganic stabilizers also yield more stable and less agglomerated ceramics.[4,12] Interestingly, the PLA/DOX/MNP carriers showed stability at pH 7.4, that is, the physiological blood pH. Stability at physiological blood pH will ensure the carriers' increased plasma half-life while traversing to the tumor site. The isoelectric points (pH_{IEP}) extrapolated from the graphs for

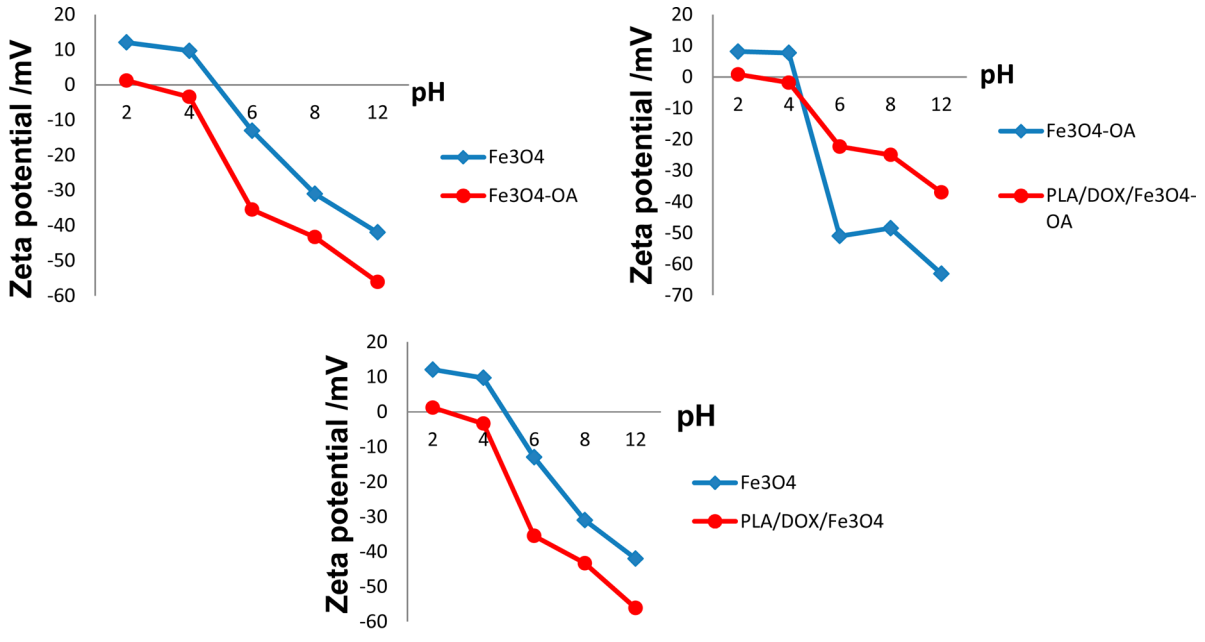

Figure 4. Zeta potential plots for Fe_3O_4, Fe_3O_4−OA, PLA/DOX/Fe_3O_4, and PLA/DOX/Fe_3O_4−OA.

DOI: 10.1021/acsami.5b07567
ACS Appl. Mater. Interfaces 2015, 7, 22692−22701

Fe_3O_4, Fe_3O_4−OA, PLA/DOX/Fe_3O_4, and PLA/DOX/Fe_3O_4−OA were 5 for Fe_3O_4 and 2 for the others. The change in pH_{IEP} can be ascribed to the inclusion of the oleic acid and PLA coating on the Fe_3O_4. Hence, stabilization of the MNPs by PLA and oleic acid is confirmed.

3.6. In Vitro Drug Release by Carriers. The % EE of DOX in the spheres was as follows: PLA/DOX/Fe_3O_4 (DCM), 57.5 ± 54.4%; PLA/DOX/Fe_3O_4 ($CHCl_3$), 59 ± 26.9%; and PLA/DOX/Fe_3O_4−OA, 59 ± 43.8% (Table 1). The DOX release from PLA/DOX/Fe_3O_4 ($CHCl_3$) followed a sustained pattern (Figure 5) and no burst effect, indicating the drug had

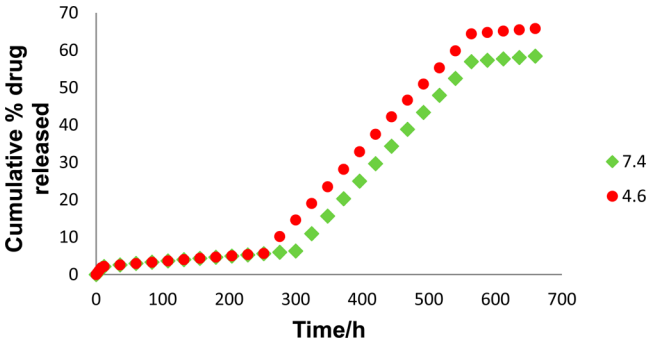

Figure 5. Cumulative release profile for PLA/DOX/MNP spheres, n = 3. The DOX release profile is sustained, prolonged and pH-dependent.

been successfully incorporated into the core of the spheres. DOX was released in three stages, as shown by the cumulative drug release plot (Figure 5). Between 0 and 276 h, only 5% of the drug was slowly released, possibly by simple diffusion, as the surrounding medium was still penetrating the PLA chains. After 276 h, a rapid and sustained DOX release was observed, which was highest at pH 4.7, reaching a plateau after 636 h. The release fitted a zero-order kinetics model and an anomalous mechanism. Table 2 shows the release constants, correlation

Table 2. Kinetics Model Correlation Coefficient (R^2), Release Constants and Release Exponent (n) for PLA/DOX/Fe_3O_4 Spheres[a]

model		7.4	4.6
zero order	R^2	0.8781	0.9112
	K_0	0.0942	0.109
first order	R^2	0.7652	0.7647
	K	0.002	0.002
Higuchi	R^2	0.7064	0.7489
	K_H	0.3084	0.2785
Korsmeyer−Peppas	R^2	0.8145	0.8092
	K_{KP}	0.815	0.7516
	n	0.8	0.8

[a] R^2 was used to determine the model that best fit the release.

coefficient, and release exponent. A zero-order release advantageously favors prolonged pharmacological action.[46] During the second stage, DOX continued to be released by simple diffusion and the gradual onset of PLA erosion affording sustained release. An anomalous mechanism has been reported for systems that release drugs through both diffusion and polymer degradation.[47] The degradation of the spheres is also confirmed by SEM images, imaged after 660 h of drug release (Figure 6). Figure 6 confirms the onset of the sphere degradation, as they showed more porosity (parts b and c) compared to the control (part a), which shows MNPs dispersed on their surfaces, perhaps blocking the pores. The prolonged DOX release from the carriers can be attributed to the strong interaction between the hydrophobic domains of PLA and the drug, causing it to be released slowly.[48] The dispersion of the MNPs within the PLA matrix can also hinder the movement of DOX through the carrier shell and thus the speed of release.[34] The PLA/MNP carriers can be used to attain sustained drug release at a targeted site, minimizing unstable plasma drug levels that could also cause side effects. The drawback of the lack of tumor-cell specificity could be addressed through magnetic modulation, delivering sufficient drug dosages at the pathological site, minimizing medical cost, and increasing patient compliance.

3.7. Cytotoxicity Studies. Figure 7 shows the proliferation percentage of the cells determined by the WST assay. Fe_3O_4 treated cells' viability increased with an increase in dosage. At high dosage (0.1 mg/mL), the NPs were agglomerated and their cell uptake was hindered. The uncoated MNPs showed pronounced cytotoxicity to the HeLa cells. However, the oleic acid coating enhanced the biocompatibility of the Fe_3O_4, evidenced by an increase in cell viability compared to uncoated Fe_3O_4. The PLA/DOX/Fe_3O_4−OA spheres showed a dosage-dependent inhibitory effect, and unlike Fe_3O_4, cell viability increased with decreasing dosage, emphasizing the stability and heterogeneous dispersion of the NPs achieved by double encapsulation (PLA and oleic acid). The PLA/DOX/Fe_3O_4 with one encapsulation modality (PLA) compared to PLA/DOX/Fe_3O_4−OA had more cell lethality, 60% cell proliferation. Nonetheless, they still showed better compatibility compared to Fe_3O_4. The PLA/DOX/MNP spheres displayed less toxicity to the HeLa cells compared to the free drug, affirming their biocompatibility and potential in biomedical application and explaining the surge in research to transfigure conventional therapeutics and attain tumor cell targeting.

3.8. Uptake of Fe_3O_4 NPs by HeLa Cells. Figure 8 show resin-embedded treated HeLa cells in HRTEM images, supporting the presence of NPs in both the extracellular (ECF) and intracellular (ICF) fluid. Cells can internalize NPs using one or more of the subsequent pathways: clathrin-mediated endocytosis (CME), micropinocytosis, phagocytosis, and caveolin-mediated endocytosis.[48] Figure 8a, region 1, shows microvilli entangled with the NPs. The arrows show movement of the NPs from the microvilli to the surface of the nucleus (region 2) and inside the nucleus (region 3). The NPs are observed enclosed in endocytic vesicles and vacuoles (Figure 8b). Hence, it is possible they were internalized by the CME and/or caveolin-mediated endocytosis and maneuvered into the nucleus via the endosome/lysosome pathway. Alternatively, they traversed into the nucleus via the endoplasmic reticulum (ER), as shown in Figure 8c,d. The NPs were observed in the endoplasmic reticulum (Figure 8d, region 4), and region 5 of the same image affirms the penetration of the nucleus envelope by the NPs. The NPs induced stress in the cells, proven by a lobed nucleus (Figure 8c). Shukla et al.[49] observed mitochondrial aberrations due to uptake of MNPs by HeLa cells. Conflictingly, the HRTEM images revealed morphological changes mainly in the nucleus. Possibly, several factors, such as the size, preparation method, and carriers, determine the uptake of the NPs, which explains the differences.

Figure 9 illustrates the proposed internalization pathway. Typically, cancer cells have increased endocytic ability due to

DOI: 10.1021/acsami.5b07567
ACS Appl. Mater. Interfaces 2015, 7, 22692−22701

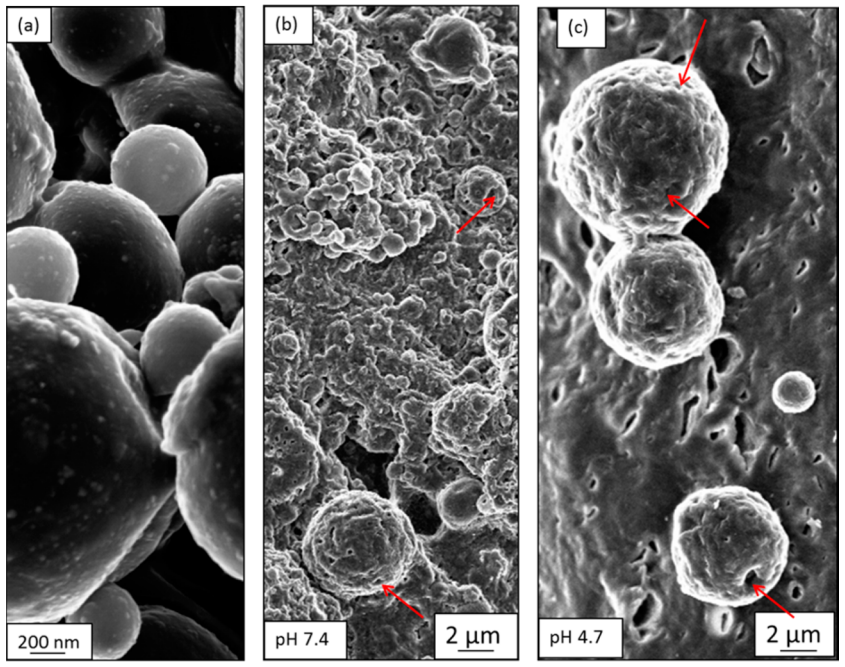

Figure 6. SEM images showing PLA/DOX/Fe_3O_4 spheres (a) control, before drug release experiment, and (b) pH 7.4 and (c) pH 4.7 spheres after 660 h of drug release. The spheres after the drug release experiment showed degradation, confirmed by porous morphology shown by red arrows, whereas in the control, the pores are blocked by the MNPs dispersed on the surface.

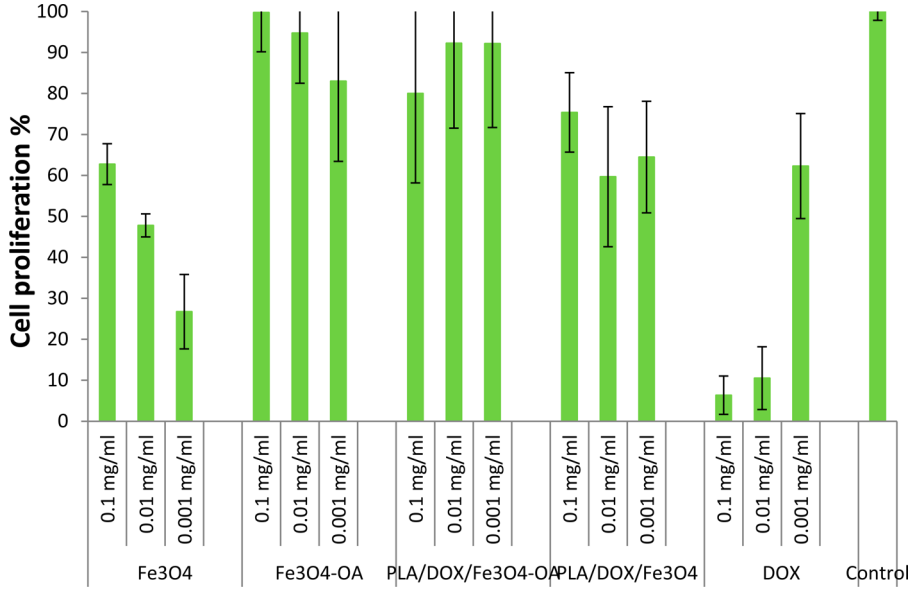

Figure 7. In vitro HeLa cell line as shown by a WST assay, illustrating the effect of Fe_3O_4, DOX, and PLA/DOX/MNP spheres on the proliferation percentage of the cells. Mean ± SD (n = 8), error bars indicate standard error of the mean, null hypothesis = 0.90 DOX cells (Student's t test).

their high metabolic and proliferation rates.[50] Once endocytosed, the NPs/carriers remain in the endocytic vesicles/vacuoles, which mature into endosomes. The endosomes will fuse with lysosomes, exposing the NPs to digestive enzymes. The enzymes will break down iron oxide into free ions, Fe^{2+} and ROS, through a Fenton reaction.[51] Successively, the lysosome will burst, empting the content into the cytosol. The free ions and ROS will traverse through the cytosol and accumulate in the nucleus and nucleolus, causing damages to the DNA, resulting in apoptosis. Alternatively, the NPs will move to the nucleus through the endoplasmic reticulum.

4. CONCLUSIONS

Improved PLA/DOX/MNP carriers for the magnetic targeting of tumor cells were successfully synthesized in our laboratory. A prolonged, pH-dependent, sustained DOX release from the system was attained; that is, the same amount of drug was released per unit time for a prolonged pharmacological action. Advantageously, through such a release, highly toxic dosages of drugs and fluctuations in the blood are eliminated, which is the downfall of conventional methods. In addition, the system exhibited no burst effect. The burst effect, which is the premature release of drug from the surface of the spheres, can result in exposure of even healthy cells to the toxic drug.

DOI: 10.1021/acsami.5b07567
ACS Appl. Mater. Interfaces 2015, 7, 22692−22701

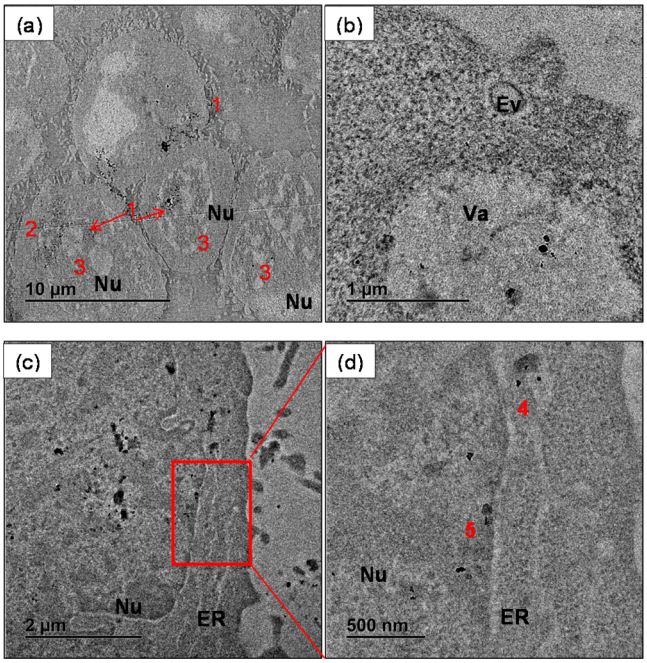

Figure 8. (a–d) TEM images of unstained HeLa cells incubated with 0.1 mg/mL PLA/DOX/Fe_3O_4 for 48 h. Abbreviations: Nu, nucleus; Mv, microvilli, EV, endocytic vesicles; Va, vacuoles; ER, endoplasmic reticulum.

However, in the absence of the burst effect, the carrier can be magnetically modulated to the site of preference where sustained release is anticipated and crucial. Through magnetic targeting, healthy cells are spared from toxic drugs, and tumor cells are concentrated with the drugs. The synthesized MNPs showed superparamagnetic properties, essential to modulating the system to tumor cells, attaining specificity and decreasing side effects, patient incompliance, and medical cost. The cytotoxicity of the PLA/DOX/MNP spheres was investigated on HeLa cells, where they showed pronounced biocompatibility after 24 h of treatment, highlighting the possibility of application in the biomedical field. Currently, we are focusing on the in vivo anticancer activity of the spheres in the absence and presence of magnetic field.

■ ASSOCIATED CONTENT

Supporting Information

The Supporting Information is available free of charge on the ACS Publications website at DOI: 10.1021/acsami.5b07567.

X-ray diffraction patterns of Fe_3O_4 and Fe_3O_4–OA nanoparticles, magnetization fields versus applied magnetic field for Fe_3O_4 nanoparticles, EDS spectra for PLA/DOX/Fe_3O_4, PLA/DOX/Fe_3O_4–OA, Fe_3O_4 and Fe_3O_4–OA, and TGA thermograms and derivative plots of Fe_3O_4, Fe_3O_4–OA, PLA/DOX/Fe_3O_4 and PLA/DOX/Fe_3O_4–OA. Finally, the mechanism of drug release from the spheres, the four empirical models discussed in this section were used to fit the in vitro release data. (PDF)

■ AUTHOR INFORMATION

Corresponding Author

*E-mail: rsuprakas@csir.co.za, suprakas73@yahoo.com.

Notes

The authors declare no competing financial interest.

■ ACKNOWLEDGMENTS

The authors are thankful to the University of Johannesburg (UJ-086310), the Council for Scientific and Industrial Research (HGER20S), the Department of Science and Technology (HGERA8X), and the National Research Foundation (NRF-78574) for financial support and laboratory facilities. We also sincerely thank the DST/CSIR National Centre for Nanostructured Materials characterization and testing facility team,

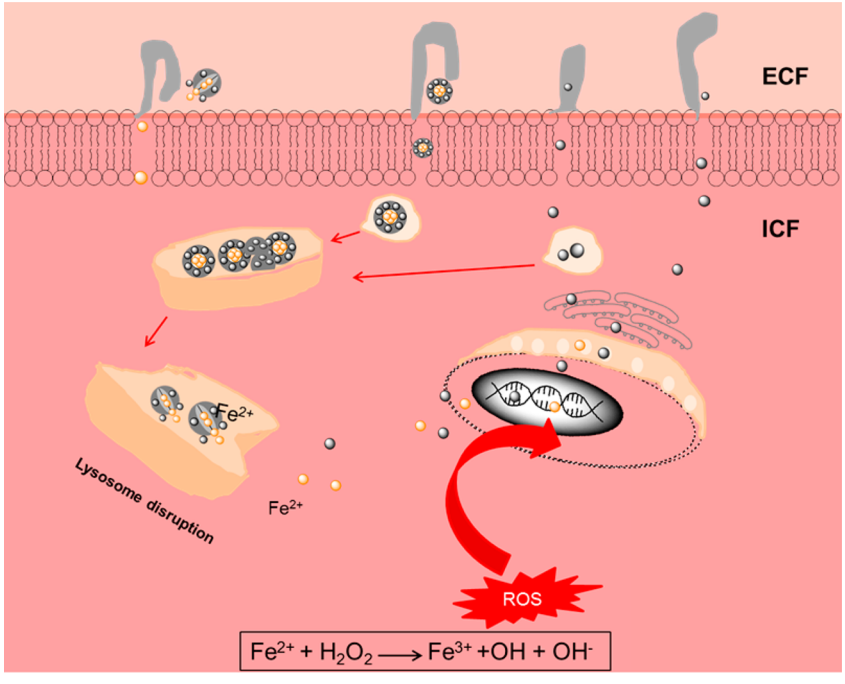

Figure 9. Sketch for a proposed mechanism of PLA/DOX/Fe_3O_4 NP cellular internalization.

DOI: 10.1021/acsami.5b07567
ACS Appl. Mater. Interfaces 2015, 7, 22692–22701

who facilitated the characterization of the nanoparticles and spheres, and Materials Science and Manufacturing for the sterile room facility.

REFERENCES

(1) Parveen, S.; Misra, R.; Sahoo, S. K. Nanoparticles: A Boom to Drug Delivery, Therapeutics, Diagnostics and Imaging. *Nanomedicine* **2012**, *8*, 147−166.

(2) Han, L.; Shi, S.; Gong, T.; Zhang, Z.; Sun, X. Cancer Stem Cells: Therapeutic Implications and Perspectives in Cancer Therapy. *Acta Pharm. Sin. B* **2013**, *3*, 65−75.

(3) Prijic, S.; Sersa, G. Magnetic Nanoparticles as Targeted Delivery Systems in Oncology. *Radiol. Oncol.* **2011**, *45*, 1−16.

(4) Chandra, S.; Barick, K. C.; Bahadur, D. Oxide and Hybrid Nanostructures for Therapeutic Applications. *Adv. Drug Delivery Rev.* **2011**, *63*, 1267−1281.

(5) Orive, G.; Hernández, R. M.; Gasc, A. R.; Pedraz, J. L. Micro and Nano Drug Delivery Systems in Cancer Therapy. *Cancer Therapy* **2005**, *3*, 131−138.

(6) Banerjee, S. S.; Chen, D. H. Magnetic Nanoparticles Grafted with Cyclodextrin for Hydrophobic Drug Delivery. *Chem. Mater.* **2007**, *19*, 6345−6349.

(7) Jain, T. K.; Reddy, M. K.; Morales, M. A.; Leslie-Pelecky, D. L.; Labhasetwar, V. Biodistribution, Clearance, and Biocompatibility of Iron Oxide Magnetic Nanoparticles in Rats. *Mol. Pharmaceutics* **2008**, *5*, 316−327.

(8) Mitra, S.; Gaur, U.; Ghosh, P. C. Tumour Targeted Delivery of Encapsulated Dextran−Doxorubicin Conjugate Using Chitosan Nanoparticles as Carrier. *J. Controlled Release* **2001**, *74*, 317−323.

(9) Jain, T. K.; Richey, J.; Strand, M.; Leslie-Pelecky, D. L.; Flask, C. A.; Labhasetwar, V. Magnetic Nanoparticles with Dual Functional Properties: Drug Delivery and Magnetic Resonance Imaging. *Biomaterials* **2008**, *29*, 4012−4021.

(10) Lai, J. J.; Hoffman, J. M.; Ebara, M.; Hoffman, A. S.; Estournés, C.; Wattiaux, A.; Stayton, P. S. Dual Magnetic-/Temperature-Responsive Nanoparticles for Microfluidic Separations and Assays. *Langmuir* **2007**, *23*, 7385−7391.

(11) Akbarzadeh, A.; Zarghami, N.; Mikaeili, H.; Asgari, D.; Goganian, A. M.; Khiabani, M.; Samiei, H. K.; Davaran, S. Synthesis, Characterization, and in vitro Evaluation of Novel Polymer-Coated Magnetic Nanoparticles for Controlled Delivery of Doxorubicin. *Nanotechnol., Sci. Appl.* **2012**, *5*, 13−25.

(12) Sun, C.; Lee, J. S. H.; Zhang, M. Magnetic Nanoparticles in MR Imaging and Drug Delivery. *Adv. Drug Delivery Rev.* **2008**, *60*, 1252−1265.

(13) Singh, N.; Jenkins, G. J. S.; Nelson, B. C.; Marquis, B. J.; Maffeis, T. G. G.; Brown, A. P.; Williams, P. M.; Wright, C. J.; Doak, S. H. The Role of Iron Redox State in the Genotoxicity of Ultrafine Superparamagnetic Iron Oxide Nanoparticles. *Biomaterials* **2012**, *33*, 163−170.

(14) Na, H. B.; Song, I. C.; Hyeon, T. Inorganic Nanoparticles for MRI Contrast Agents. *Adv. Mater.* **2009**, *21*, 2133−2148.

(15) Thomas, R.; Park, I.-K.; Jeong, Y. Magnetic Iron Oxide Nanoparticles for Multimodal Imaging and Therapy of Cancer. *Int. J. Mol. Sci.* **2013**, *14*, 15910−15930.

(16) Huang, H. S.; Hainfeld, J. F. Intravenous Magnetic Nanoparticle Cancer Hyperthermia. *Int. J. Nanomed.* **2013**, *8*, 2521−2532.

(17) Bañobre-Lõpez, M.; Teijeiro, A.; Rivas, J. Magnetic Nanoparticle-Based Hyperthermia for Cancer Treatment. *Rep. Pract. Oncol. Radiother.* **2013**, *18*, 397−400.

(18) Hsing, I.; Xu, Y.; Zhao, W. Micro- and Nano-Magnetic Particles for Applications in Biosensing. *Electroanalysis* **2007**, *19*, 755−768.

(19) Kutushov, M. V.; Kuznetsov, A. A.; Filippov, V. I.; Kuznetsov, O. A. *Scientific and Clinical Applications of Magnetic Carriers*; Plenum Press: New York, 1997; pp 391−397.

(20) Oh, J. K.; Park, J. M. Iron Oxide-based Superparamagnetic Polymeric Nanomaterials: Design, Preparation, and Biomedical Application. *Prog. Polym. Sci.* **2011**, *36*, 168−189.

(21) Veiseh, O.; Gunn, J. W.; Zhang, M. Design and Fabrication of Magnetic Nanoparticles for Targeted Drug Delivery and Imaging. *Adv. Drug Delivery Rev.* **2010**, *62*, 284−304.

(22) Chomoucka, J.; Drbohlavova, J.; Huska, D.; Adam, V.; Kizek, R.; Hubalek, J. Magnetic Nanoparticles and Targeted Drug Delivering. *Pharmacol. Res.* **2010**, *62*, 144−149.

(23) Li, F.; Li, X.; Li, B. Preparation of Magnetic Polylactic Acid Microspheres and Investigation of its Releasing Property for Loading Curcumin. *J. Magn. Magn. Mater.* **2011**, *323*, 2770−2775.

(24) Jia, Y.; Yuan, M.; Yuan, H.; Huang, H.; Sui, X.; Cui, X.; Tang, F.; Peng, J.; Chen, J.; Lu, S.; Xu, W.; Zhang, L.; Guo, Q. Co-encapsulation of Magnetic Fe_3O_4 Nanoparticles and Doxorubicin into Biodegradable PLGA Nanocarriers for Intratumoral Drug Delivery. *Int. J. Nanomed.* **2012**, *7*, 1697−1708.

(25) Yang, J.; Park, S.-B.; Yoon, H.; Huh, Y.-M.; Haam, S. Preparation of Poly(ε-caprolactone) Nanoparticles Containing Magnetite for Magnetic Drug Carrier. *Int. J. Pharm.* **2006**, *324*, 185−190.

(26) Hortobágyi, G. N. Anthracyclines in the Treatment of Cancer: An Overview. *Drugs* **1997**, *54*, 1−7.

(27) Goodman, M. F.; Lee, G. M. Adriamycin Interactions with T4 DNA Polymerase: Two Modes of Template-Mediated Inhibition. *J. Biol. Chem.* **1977**, *252*, 2670−2674.

(28) Yousefpour, P.; Atyabi, F.; Farahani, E. V.; Sakhtianchi, R.; Dinarvand, R. Polyanionic Carbohydrate Doxorubicin-Dextran Nanocomplex as a Delivery System for Anticancer Drugs: In Vitro Analysis and Evaluations. *Int. J. Nanomed.* **2011**, *6*, 1487−1496.

(29) Feng, T.; Tian, H.; Xu, C.; Lin, L.; Xie, Z.; Lam, M. H.; Liang, H.; Chen, X. Synergistic Co-Delivery of Doxorubicin and Paclitaxel by Porous PLGA Microspheres for Pulmonary Inhalation Treatment. *Eur. J. Pharm. Biopharm.* **2014**, *88*, 1086−1093.

(30) Cui, Y.; Xu, Q.; Chow, P. K.; Wang, D.; Wang, C. Transferrin-conjugated magnetic silica PLGA nanoparticles loaded with doxorubicin and paclitaxel for brain glioma treatment. *Biomaterials* **2013**, *34*, 8511−8520.

(31) Narayanan, S.; Mony; Vijaykumar, K. D.; Koyakutty, M.; Paul-Prasanth, B.; Menon, D. Sequential Release of Epigallocatechin Gallate and Paclitaxel from PLGA Casein Core/Shell Nanoparticles Sensitizes Drug-Resistant Breast Cancer Cells. *Nanomedicine* **2015**, *11*, 1399−1406.

(32) Alibolandi, M.; Sadeghi, F.; Abnous, K.; Atyabi, F.; Ramezani, M.; Hadizadeh, F. The Chemotherapeutic Potential of Doxorubicin-Loaded PEG-b-PLGA Nanopolymersomes in Mouse Breast Cancer Model. *Eur. J. Pharm. Biopharm.* **2015**, *94*, 521−531.

(33) Ma, M.; Zhang, Y.; Yu, W.; Shen, H.; Zhang, H.; Gu, N. Preparation and Characterization of Magnetite Nanoparticles Coated by Amino Silane. *Colloids Surf., A* **2003**, *212*, 219−226.

(34) Zhang, X.; Xue, L.; Wang, J.; Liu, Q.; Liu, J.; Gao, Z.; Yang, W. Effects of Surface Modification on the Properties of Magnetic Nanoparticles/PLA Composite Drug Carriers and in vitro Controlled Release Study. *Colloids Surf., A* **2013**, *431*, 80−86.

(35) Qu, H.; Caruntu, D.; Liu, H.; O'Connor, C. J. Water-Dispersible Iron Oxide Magnetic Nanoparticles with Versatile Surface Functionalities. *Langmuir* **2011**, *27*, 2271−2278.

(36) Lan, Q.; Liu, C.; Yang, F.; Liu, S.; Xu, J.; Sun, D. Synthesis of Bilayer Oleic Acid-Coated Fe_3O_4 Nanoparticles and Their Application in pH-responsive Pickering Emulsions. *J. Colloid Interface Sci.* **2007**, *310*, 260−269.

(37) Zhao, S. Y.; Lee, D. K.; Kim, C. W.; Cha, H. G.; Kim, Y. H.; Kang, Y. S. Synthesis of Magnetic Nanoparticles of Fe_3O_4 and $CoFe_2O_4$ and Their Surface Modification by Surfactant Adsorption. *Bull. Korean Chem. Soc.* **2009**, *27*, 237−242.

(38) Gupta, A. K.; Gupta, M. Synthesis and Surface Engineering of Iron Oxide Nanoparticles for Biomedical Applications. *Biomaterials* **2005**, *26*, 3995−4021.

(39) Mahdavi, M.; Ahmad, M. B.; Haron, M. J.; Namvar, F.; Nadi, B.; Rahman, M. Z. A. B.; Amin, J. Synthesis, Surface Modification and Characterisation of Biocompatible Magnetic Iron Oxide Nanoparticles for Biomedical Applications. *Molecules* **2013**, *18*, 7533−7548.

DOI: 10.1021/acsami.5b07567
ACS Appl. Mater. Interfaces 2015, 7, 22692−22701

(40) Hoa, L. T. M.; Dung, T. T.; Danh, T. M.; Duc, N. H.; Chien, D. M. Preparation and Characterization of Magnetic Nanoparticles Coated with Polyethylene Glycol. *J. Phys. Conf. Ser.* **2009**, *187*, 012048.
(41) Andrade, A. L.; Souza, D. M.; Pereira, M. C.; Fabris, J. D.; Domingues, R. Z. Synthesis and Characterization of Magnetic Nanoparticles Coated with Silica Through a Sol-Gel Approach. *Ceramica* **2009**, *55*, 420−424.
(42) Kayal, S.; Ramanujan, R. V. Doxorubicin Loaded PVA Coated Iron Oxide Nanoparticles for Targeted Drug Delivery. *Mater. Sci. Eng., C* **2010**, *30*, 484−490.
(43) Zhang, Y.; Yang, M.; Portney, N. G.; Cui, D.; Budak, G.; Ozbay, E.; Ozkan, M.; Ozkan, C. S. Zeta Potential: A Surface Electrical Characteristic to Probe the Interaction of Nanoparticles with Normal and Cancer Human Breast Epithelial Cells. *Biomed. Microdevices* **2008**, *10*, 321−328.
(44) Xu, R. *Particle Characterization: Light Scattering Methods*. Kluwer Academic Publishers: Greenbelt, 2001.
(45) Lübbe, A. S.; Bergemann, C.; Huhnt, W.; Fricke, T.; Riess, H.; Brock, J. W.; Huhn, D. Preclinical Experiences with Magnetic Drug Targeting: Tolerance and Efficacy. *Cancer Res.* **1996**, *56*, 4694−4701.
(46) Costa, P.; Sousa Lobo, J. M. Modeling and Comparison of Dissolution Profiles. *Eur. J. Pharm. Sci.* **2001**, *13*, 123−133.
(47) Sanna, V.; Roggio, A. M.; Posadino, A. M.; Cossu, A.; Marceddu, S.; Mariani, A.; Alzari, V.; Uzzau, S.; Pintus, G.; Sechi, M. Novel Docetaxel-Loaded Nanoparticles Based on Poly(lactide-co-caprolactone) and Poly(lactide-co-glycolide-co-caprolactone) for Prostate Cancer Treatment: Formulation, Characterization, and Cytotoxicity Studies. *Nanoscale Res. Lett.* **2011**, *6*, 260−266.
(48) Zhu, J.; Liao, L.; Zhu, L.; Zhang, P.; Guo, K.; Kong, J.; Ji, C.; Liu, B. Size-Dependent Cellular Uptake Efficiency, Mechanism, and Cytotoxicity of Silica Nanoparticles Toward HeLa Cells. *Talanta* **2013**, *107*, 408−415.
(49) Shukla, S.; Jadaun, A.; Arora, V.; Sinha, R. K.; Biyani, N.; Jain, V. K. *In vitro* Toxicity Assessment of Chitosan Oligosaccharide Coated Iron Oxide Nanoparticles. *Toxicol. Rep.* **2015**, *2*, 27−39.
(50) Prijic, S.; Sersa, G. Magnetic Nanoparticles as Targeted Delivery Systems in Oncology. *Radiol. Oncol.* **2011**, *45*, 1−16.
(51) Singh, N.; Jenkins, G. J. S.; Asadi, R.; Doak, S. H. Potential Toxicity of Superparamagnetic Iron Oxide Nanoparticles (SPION). *Nano Rev.* **2010**, *1*, 5358.

DOI: 10.1021/acsami.5b07567
ACS Appl. Mater. Interfaces 2015, 7, 22692−22701